Fabrication, Characterization, and Optical Properties of Gold Nanoparticle/Porous Alumina Composites: The Nonscattering Maxwell−Garnett Limit

Gabor L. Hornyak, Charles J. Patrissi, and Charles R. Martin*

Department of Chemistry, Colorado State University, Fort Collins, Colorado 80523-1872

Received: August 30, 1996; In Final Form: December 12, 1996[⊗]

We have been exploring the optical properties of nanoscopic gold particles prepared by electrochemically depositing Au within the pores of nanoporous alumina membranes. Maxwell−Garnet (MG) effective medium theory has been used as a guide for modeling the optical properties of these Au nanoparticle/alumina membrane composites. MG theory is, however, rigorously applicable only in the limit of metal nanoparticles with infinitesimally small diameters. As a result, the position of the plasmon resonance absorption predicted theoretically using MG theory was always blue-shifted relative to the position of the experimental absorption band. The smallest diameter particles investigated in this prior work had diameters of 60 nm. Au nanoparticles with smaller diameters (52 nm down to 16 nm) were prepared, and the optical properties of composites containing these nanoparticles are described here. The λ_{max} values for the smallest diameter particles are essentially identical with the values predicted by MG theory. Hence, we have succeeded in preparing Au nanoparticles that experimentally achieve the MG-predicted plasmon resonance absorption limit.

Introduction

We[1,2] and others[3] have been investigating the properties of nanomaterials prepared within the pores of nanoporous alumina membranes. These membranes are prepared electrochemically from aluminum metal and contain monodisperse, cylindrical pores that are packed into a regular hexagonal array.[1−4] The diameter of the pores in these membranes can be varied by controlling the potential used during the electrochemical preparation. In addition, these membranes are highly optically transparent, which makes them ideal for visible spectroscopic characterization of nanoparticles deposited within the pores of these membranes.[2]

We have been exploring the optical properties of nanoscopic gold particles prepared by electrochemically depositing Au within the pores of such alumina membranes.[1,2] In particular, we are interested in investigating the effect of Au nanoparticle diameter (determined by the pore diameter of the alumina membrane) and length (determined by the quantity of Au deposited within the pores) on the position of the plasmon resonance adsorption of the nanoparticle.[2] We have used Maxwell−Garnet (MG) effective medium theory as a guide for modeling the optical properties of these Au nanoparticle/alumina membrane composites.[2] MG theory is, however, rigorously applicable only in the limit of metal nanoparticles with infinitesimally small diameters. As a result, the position of the plasmon resonance absorption predicted theoretically using MG theory was always blue-shifted relative to the position of the experimental absorption band.[2a,b] We have developed a modified form of MG theory, called the *dynamic* MG (DMG) theory, to model the optical properties of such Au nanoparticles.[2b]

In our previous studies we found that as the diameter of the Au nanoparticle decreased, the position of the experimental plasmon resonance band (as defined by the wavelength of maximum absorption intensity, λ_{max}) approached the λ_{max} predicted by MG theory.[2b] The smallest diameter particles investigated in our previous study had diameters of 60 nm.[2b] We have since prepared Au nanoparticles with even smaller diameters (52 nm down to 16 nm). We have found, again, that as the Au nanoparticle diameter decreases, the experimental λ_{max} approaches the MG-predicted value. Furthermore, the λ_{max} values for the smallest diameter particles (16 nm) are essentially identical with the values predicted by MG theory. Hence, we have succeeded in preparing Au nanoparticles which experimentally achieve the MG-predicted plasmon resonance absorption limit. The results of these investigations are described here.

Experimental Section

Preparation of the Nanoporous Alumina Template Membranes. The template membranes were prepared by anodizing high-purity (>99.999%) aluminum (Reynolds). Prior to anodization, the Al was rerolled by PV&D Research Materials Inc. to a thickness of 1 mm. Anodes of dimensions 8 × 10 cm were cut from this Al sheet. The anodes were degreased in a 1:2:1 (by volume) ethanol−dichloromethane−acetone solution and then rinsed with acetone and distilled water. The anodes were then etched in 0.05 M NaOH for 10 min, rinsed in purified water, 50% (w/w) nitric acid, and then water again. The purified water was obtained by passing house-distilled water through a Milli-Q (Millipore) water-purification system. This water was used for all aqueous solutions.

The Al anodes were then electropolished in a 2:3 (v/v) phosphoric/sulfuric acid solution that was 1% in glycerol. An electropolishing current density of ca. 75 mA/cm^2 was used, and the cell was maintained at a temperature of 70−80 °C.[5] Convection was provided by nitrogen gas bubbling and by mechanical stirring. Polishing was done for approximately 10 min until a mirror finish was obtained. The electropolished Al was rinsed immediately in distilled water (often requiring a strong stream to remove the tenacious gelatinous oxide layer), immersed in concentrated nitric acid for 10 min, rinsed, and left to dry in air.

The pretreated Al was then anodized at constant potential which converts the surface into the desired nanoporous alumina template membrane. The method and cell have been described previously.[2b,c] The diameter of the pores obtained in the alumina membrane depends on the anodization potential. The potentials

* Corresponding author: crmartin@lamar.colostate.edu.
[⊗] Abstract published in *Advance ACS Abstracts,* February 1, 1997.

S1089-5647(96)02685-5 CCC: $14.00

TABLE 1: Conditions Used for Electrochemical Preparation of the Nanoporous Alumina Membranes and Characteristics of the Resulting Membranes

applied dc potential (V)	anodization time (h)	electrolyte and concn (% w/w)	detaching acid and concn(% w/w)	pore diam (nm)
30	12	oxalic acid (4%)	phosphoric acid (25%)	52
20	4	sulfuric acid (10%)	sulfuric acid (25%)	32
15	6	sulfuric acid (10%)	sulfuric acid (25%)	22
10	10	sulfuric acid (15%)	sulfuric acid (25%)	16

TABLE 2: Conditions Used to Electrodeposit the Au Nanoparticles and Characteristics of the Resulting Nanoparticles

membrane pore diam (nm)	plating coulombs used[a]	Au particle diam (nm)	Au particle length (nm)	aspect ratio	κ
52	0.10	52 ± 6	68 ± 14	1.3	1.71
	0.20		142 ± 20	2.7	1.27
	0.40		406 ± 110	7.8	1.06
32	0.05	32 ± 4	32 ± 4	1.0	1.99
	0.10		48 ± 10	1.5	1.60
	0.20		80 ± 30	2.5	1.32
	0.30		138 ± 56	4.3	1.15
	0.50		208 ± 90	6.5	1.08
	0.56		370 ± 70	12	1.04
22	0.05	22 ± 2	26 ± 2	1.2	1.81
	0.40		54 ± 14	2.5	1.31
	0.50		68 ± 12	3.1	1.22
	1.00		110 ± 40	5.0	1.11
	1.50		316 ± 60	14	1.02
16	0.13	16 ± 2	36 ± 10	2.3	1.34
	0.54		96 ± 38	6.0	1.08
	0.42		300 ± 130	19	1.01

[a] Area of membrane exposed to solution = 3.14 cm^2.

and electrolytes used to produce the membranes studied here are shown in Table 1. To avoid a large current surge, the potential was ramped over a period of 2 min to the final values indicated in Table 1. The cell was maintained at ca. 5 °C during anodization. The thicknesses of the membranes obtained varied from 20 to 40 μm.

The alumina membrane was removed from the substrate Al anode using the voltage reduction technique.[6] This entails stepwise reduction of the potential to obtain an interfacial oxide layer that has a network of much smaller pores. After formation of this highly porous layer, the electrode was immersed into an acidic detachment solution (Table 1) which results in rapid dissolution of the interfacial oxide. The acid then has access to the substrate Al, and H_2 gas is evolved at the interface between the Al and the alumina membrane. The evolving H_2 gas bubbles can be seen through the transparent alumina membrane. When these bubbles coalesce, detachment is complete. The Al electrode (with the detached alumina membrane still clinging to the surface) was removed from the detaching solution, rinsed by immersion into three portions of water and dried in air. The membrane was collected by sliding an index card between the alumina and the substrate Al. The Al electrode can then be used to prepare another alumina membrane.

The two faces of the detached alumina membrane are not equivalent. The face that was detached from the substrate Al surface contains remnants of the interfacial oxide layer. This was removed by floating the membrane onto the surface of a 0.2 M KOH solution in ethylene glycol. This makes both faces of the membrane essentially equivalent. The membranes were checked visually for optical clarity. Defects on the Al metal surface such as pits and scratches produce defects in the oxide membrane which scatter light. Such defective membranes were discarded.

Gold Particle Electrodeposition. The nanoscopic Au particles were obtained by electrodepositing gold within the pores

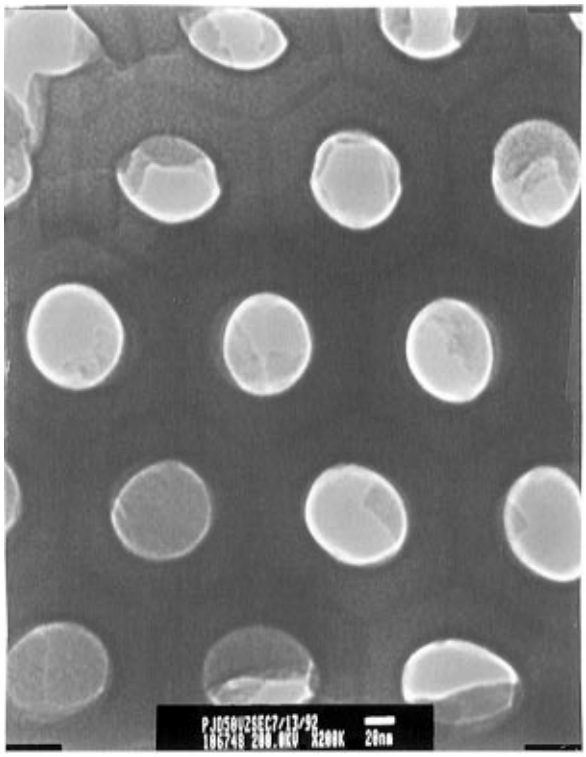

Figure 1. Transmission electron micrograph of a planar section of a typical nanoporous alumina membrane.

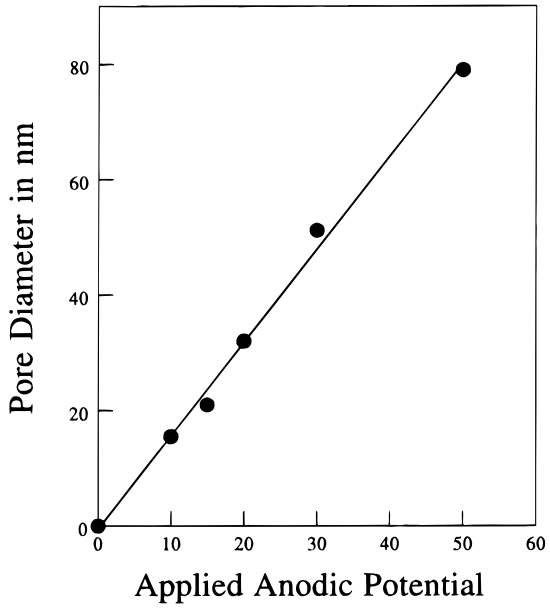

Figure 2. Variation of pore diameter in the nanoporous alumina membranes with voltage used during anodization.

of the alumina membranes. The procedure used has been described previously.[2c] Briefly, a thin (ca. 100 nm) layer of Ag was first evaporated onto the KOH/glycol-etched face of the membrane. The Ag film was used to electrodeposit Ag "nanopedestals" into the pores of the membrane. The Au nanoparticles were then deposited onto these Ag pedestals. This

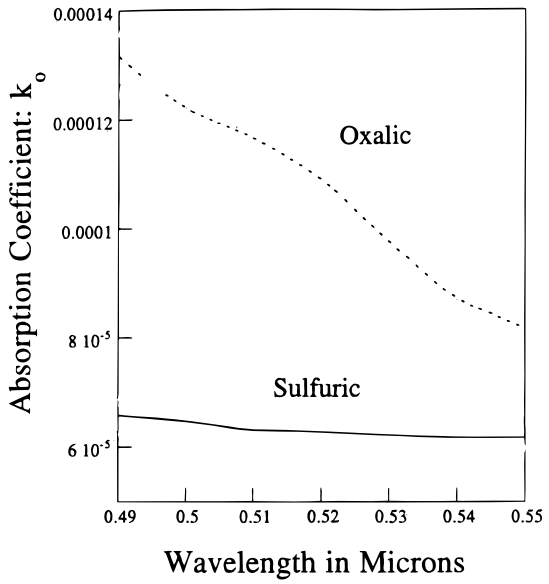

Figure 3. Plot of the wavelength-dependent k_0 for the alumina membranes vs wavelength**.** Upper curve is for membranes prepared in oxalic acid; lower curve is for membranes prepared in sulfuric acid (Table 1).

approach was used because it puts the Au nanoparticles into the bulk of the alumina membrane where the pore diameter is more uniform. The Ag was then dissolved by immersion of the membrane into concentrated nitric acid.

Because of the cylindrical pore geometry, rod-shaped Au nanoparticles were obtained. The diameter of these rod-shaped particles is determined by the pore diameter. The aspect ratio (length divided by diameter) is determined by the quantity of Au deposited (Table 2). It is important to point out, however, that not all of the electroplated Au is deposited within the pores. For example, an O-ring is used to hold the membrane in place in the electrochemical cell, and the portion of the membrane directly under this O-ring is typically completely covered with a visible layer of Au. This is due to the pressure exerted from the O-ring, which creates cracks in the membrane. Hence, the current efficiency for plating of the Au within the pores was always less than unity. This is not, however, a problem because the lengths and diameters of the Au nanoparticles were measured using transmission electron microscopy (Table 2).[2]

Spectrophotometric Investigations. UV/visible absorption data were obtained using a transmission-mode experiment on the Au nanoparticle/alumina membrane composite. The method used has been described previously.[2b] Optical data on the alumina membrane, before deposition of the Au nanoparticles, were used to obtain the refractive index (n_0) and the absorption coefficient (k_0) for the membrane. The method used is reviewed in the Theory section. After deposition of the Au nanoparticles, the membranes show a strong absorption in the visible region called the plasmon resonance band. This absorption is the focus of this paper.

Transmission Electron Microscopy (TEM). TEM images were obtained using a JEOL 2000 electron microscope. An ultramicrotome equipped with a diamond knife was used to cut thin transverse and planar sections through the Al/alumina composite membrane. The transverse sections show the length and diameter of the Au nanoparticles. These data are collected in Table 2. The planar sections show the particle diameter. In addition, planar sections of the membrane, prior to deposition of Au, were used to evaluate the porosity of these membranes. Details of the TEM procedures can be found in ref 7.

Computer Simulations. The energy of the plasmon resonance band (as defined by the wavelength of maximum absorption, λ_{max}) is determined by both the diameter and length of the Au nanoparticles deposited within the template membrane.[2] The objective of the computer simulations was to calculate the absorption spectra for the various Au nanoparticle/alumina membrane composites. These calculated spectra were then compared to the experimental spectra. We are particularly interested in the extent of agreement between the calculated and experimental λ_{max} values. Alumina optical constants were obtained experimentally and those for Au were taken from the literature.[8] The computational methods are described in the Theory section. Simulations were done using MatLab version 4.2c.1 (Mathworks, Inc.) software running on a Power Mac 7200/90 personal computer (Macintosh). Kaleidagraph (Abelbeck Software) was used to convert both the simulated and experimental absorption data to the spectral format presented in this paper.

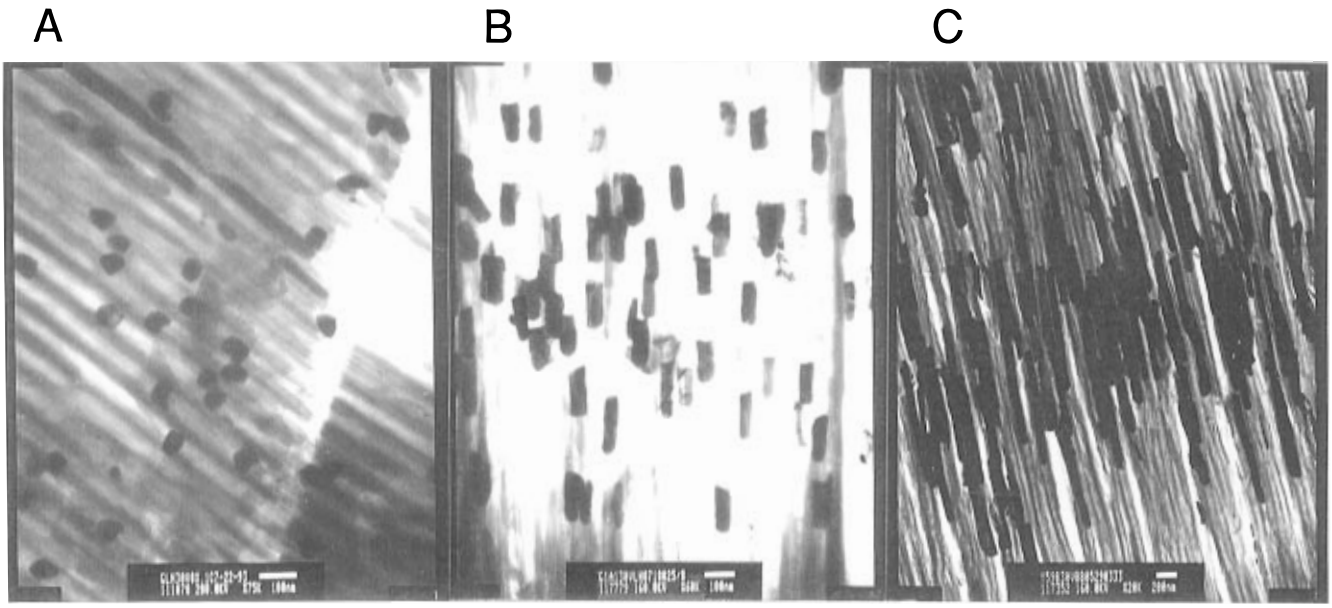

Figure 4. Transmission electron micrographs of transverse sections of Au nanoparticle/alumina membrane composites. The membranes had a pore diameter of 52 nm. The magnification and the length of the scale bar on the image are given in parentheses below. (A) Aspect ratio = 1.3 nanoparticles (×75K, 100 nm). (B) Aspect ratio = 2.7 nanoparticles (×60K, 100 nm). (C) Aspect ratio = 7.8 nanoparticles (×20K, 200 nm).

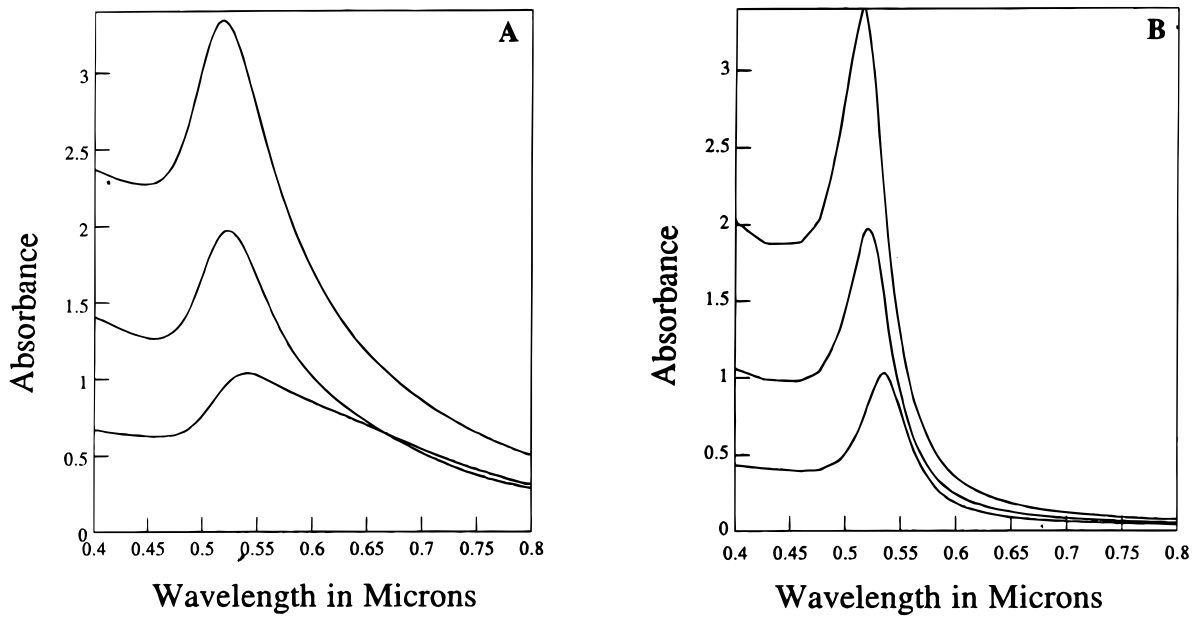

Figure 5. Experimental (A) and DMG-simulated (B) absorption spectra for membranes containing 52 nm diameter Au nanoparticles. Particles with three different aspect ratios (Table 2) are shown. The uppermost curve is for the highest aspect ratio nanoparticle, and the lowermost curve is for the lowest aspect ratio nanoparticle.

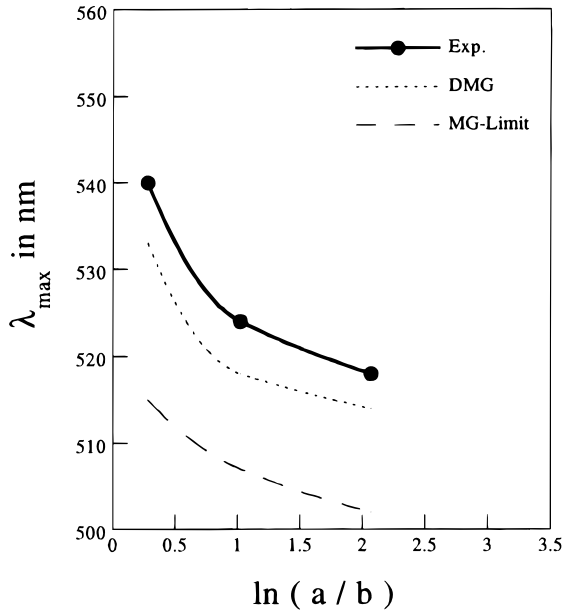

Figure 6. Plot of λ_{max} for experimental and simulated absorption spectra vs natural logarithm of the aspect ratio of the Au nanoparticle. The aspect ratio is defined as a/b, where a is the length and b is the diameter of the nanoparticle. These data are for 52 nm diameter nanoparticles. The experimental data are in bold (with data points). The DMG-simulated results are the dotted curve. The MG-simulated results are the dashed curve.

Theory

Maxwell−Garnett Theory. We have previously shown that Maxwell−Garnett (MG) effective medium theory can be used to qualitatively describe the absorption spectra of Au/alumina composite membranes of the type described here.[2] MG theory assumes that the radius of the Au nanoparticle is infinitesimally small relative to the wavelength of light.[9−11] This is called the "quasistatic" regime, and Kreibig and Vollmer specify that this regime is characterized by $r/\lambda \leq 0.01$,[11] where r is the radius of the metal nanoparticle and λ is the wavelength of light employed. According to MG theory, the complex dielectric function of the composite ($\tilde{\epsilon}_\chi$), at any λ, is related to the dielectric functions of the alumina ($\tilde{\epsilon}_0$) and the Au ($\tilde{\epsilon}_\mu$) via

$$\frac{\tilde{\epsilon}_c - \tilde{\epsilon}_0}{\tilde{\epsilon}_c + \kappa\tilde{\epsilon}_0} = f_m\left(\frac{\tilde{\epsilon}_m - \tilde{\epsilon}_0}{\tilde{\epsilon}_m + \kappa\tilde{\epsilon}_0}\right) \quad (1)$$

where f_m is the volume fraction of the Au in the composite, and κ is the shape-dependent screening parameter.[9−12] For eq 1 to be valid, f_m must be significantly less than the alumina volume fraction, f_0.[13]

The magnitude of the radius of the Au nanoparticle does not enter into eq 1 because, as noted above, MG theory assumes that the radius is infinitesimally small. However, the shape and orientation of the particle determine the value of the screening parameter, κ. For example, κ has a value of 2 for a spherical particle and a value of unity for an infinitely long, needlelike particle oriented perpendicular to the electric field.[12b] κ values were calculated, as described in ref 2b, from the known diameter and length of the nanoparticles (Table 2). Equation 1 can then be used to calculate the complex dielectric function of the composite at any λ, and this, in turn, can be used to calculate the absorption at any wavelength. The methods used have been described previously.[2b,c]

In our prior work,[2a,b] we could not achieve this quasi-static regime because the diameters of the Au nanoparticles were not infinitesimally small relative to the wavelengths of visible light. (The prior work involved Au particles with diameters ranging from 60 to 120 nm.) As a result, the λ_{max} values in the experimental absorption spectra were always greater than those calculated using MG theory. A modified version of MG theory, that takes into account the finite diameter of the Au nanoparticle, was developed.[2b] In this dynamic Maxwell−Garnett (DMG) model, the static κ of eq 1 is replaced by a complex and wavelength-dependent k_{eff}, which accounts for extinction due to scattering by the larger particles.[2b,14] Details of the DMG theory can be found in ref 2b.

Alumina Optical Constants. There are no data tables available in the literature listing the wavelength-dependent optical constants for alumina of the type used here. (These membranes consist of hydrated amorphous alumina into which some anodization electrolyte has been incorporated[4a,f]). To

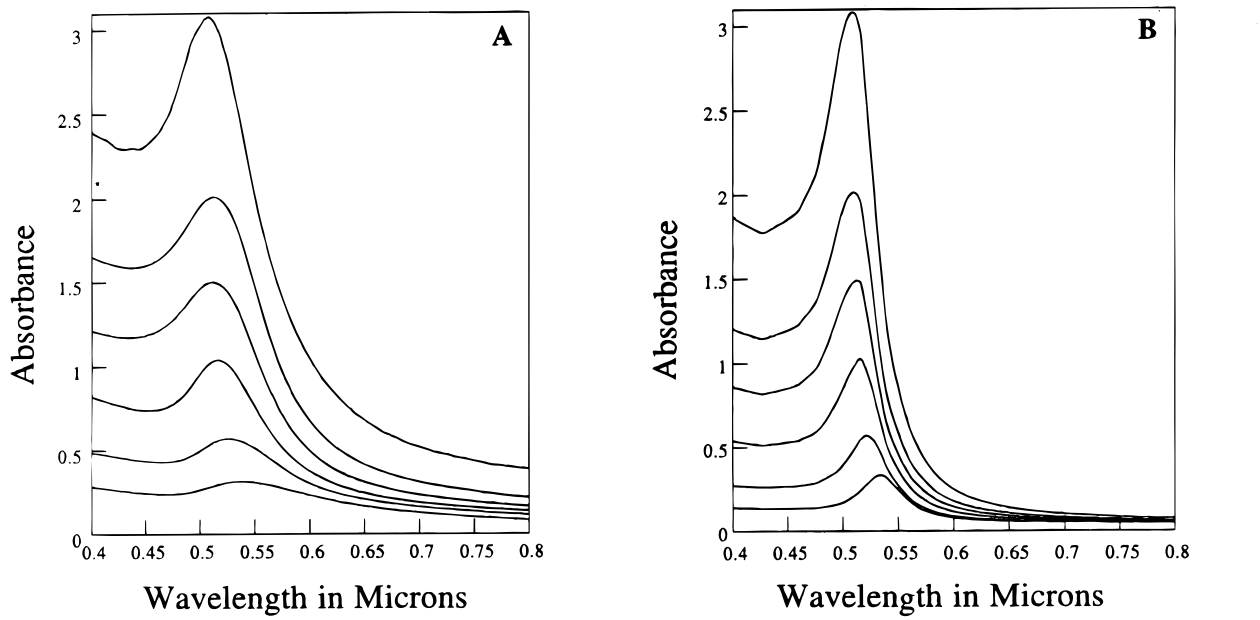

Figure 7. Experimental (A) and DMG-simulated (B) absorption spectra for membranes containing 32 nm diameter Au nanoparticles. Particles with six different aspect ratios (Table 2) are shown. The uppermost curve is for the highest aspect ratio nanoparticle, and the lowermost curve is for the lowest aspect ratio nanoparticle.

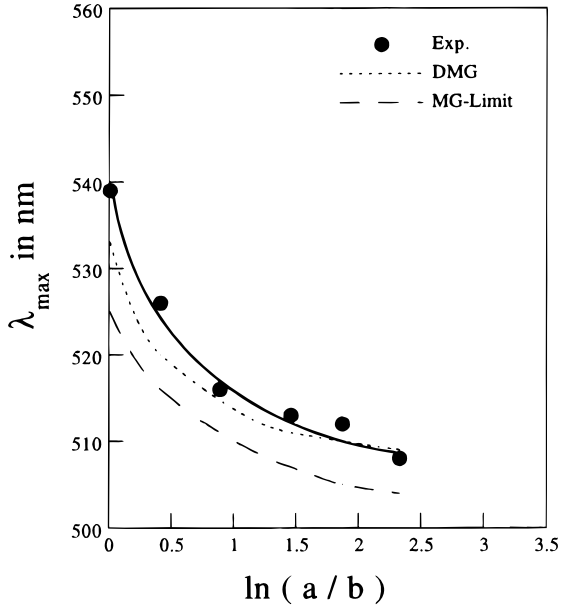

Figure 8. Plot of λ_{max} for experimental and simulated absorption spectra vs natural logarithm of the aspect ratio of the Au nanoparticle. The aspect ratio is defined as a/b, where a is the length and b is the diameter of the nanoparticle. These data are for 32 nm diameter nanoparticles. The experimental data are in bold (with data points). The DMG-simulated results are the dotted curve. The MG-simulated results are the dashed curve.

obtain accurate optical data for use in spectral modeling of the composites, we needed to determine n_0 and k_0 for these alumina membranes. This is not as simple as it seems because the membrane, itself, is a composite of alumina and the air-filled pores. Hence, two sets of optical constants can be defined for the membrane, n_0 and k_0, which are the optical constants of the alumina portion of the membrane, and n_c and k_c, which are the optical constants of the alumina/air composite. The alumina/air composite constants are obtained experimentally, and the alumina constants can then be extracted from these experimental data.

The optical constants n_c and k_c were obtained by measuring the transmittance of membranes of at least three thicknesses and applying the following equation at each wavelength:

$$\ln T_{c(i,j)} = 2 \ln\left[1 - \frac{(n_{c(i,j)} - 1)^2 + k_{c(i,j)}^2}{(n_{c(i,j)} + 1)^2 + k_{c(i,j)}^2}\right] - \frac{4\pi k_{c(i,j)} d_i}{\lambda_j} \quad (2)$$

where $T_{c(i,j)}$ is the transmittance of an alumina/air composite of some thickness (d_i in microns) at some wavelength (λ_i in microns). According to eq 2, a plot of ln $T_{c(i,j)}$ versus membrane thickness is linear; k_c is obtained from the slope and n_c from the intercept.

The alumina optical constants were obtained from these experimental n_c and k_c values using the Bruggeman approximation,[15] another type of effective medium theory, which for this specific case, takes the form

$$0 = f_0\left(\frac{\tilde{\epsilon}_0 - \tilde{\epsilon}_c}{\tilde{\epsilon}_0 + \tilde{\epsilon}_c}\right) + P\left(\frac{1 - \tilde{\epsilon}_c}{1 + \tilde{\epsilon}_c}\right) \quad (3)$$

where $\tilde{\epsilon}_0$ and $\tilde{\epsilon}_\chi$ are the complex dielectric functions of the alumina and the air/alumina composite membrane, respectively, f_0 is the volume fraction of the alumina, and P is the porosity ($1 - f_0$). This expression is solved for $\tilde{\epsilon}_0$ for each desired λ, and $\tilde{\epsilon}_0$ is then converted into the optical constants n_0 and k_0.[2b,c]

Results and Discussion

Membranes. A TEM image of a planar-section of a typical nanoporous alumina membrane is shown in Figure 1. These membranes have monodisperse pore diameters, and the pores are hexagonally packed. The pore diameter is proportional to the dc potential used to prepare the membrane (Figure 2).[16] The pore diameters for the membranes investigated here are shown in Table 1. The porosity of the membrane (P) was also determined from TEMs such as that shown in Figure 1. The porosity was found to be $P = 0.27 + 0.03$, independent of pore diameter.

As discussed in the Experimental and Theory sections, optical constants n_0 and k_0 were measured for the alumina component of the membranes used here. Figure 3 shows the variation in k_0 with wavelength, over the wavelength region of interest for these studies. The k_0 values for all membranes are quite low,

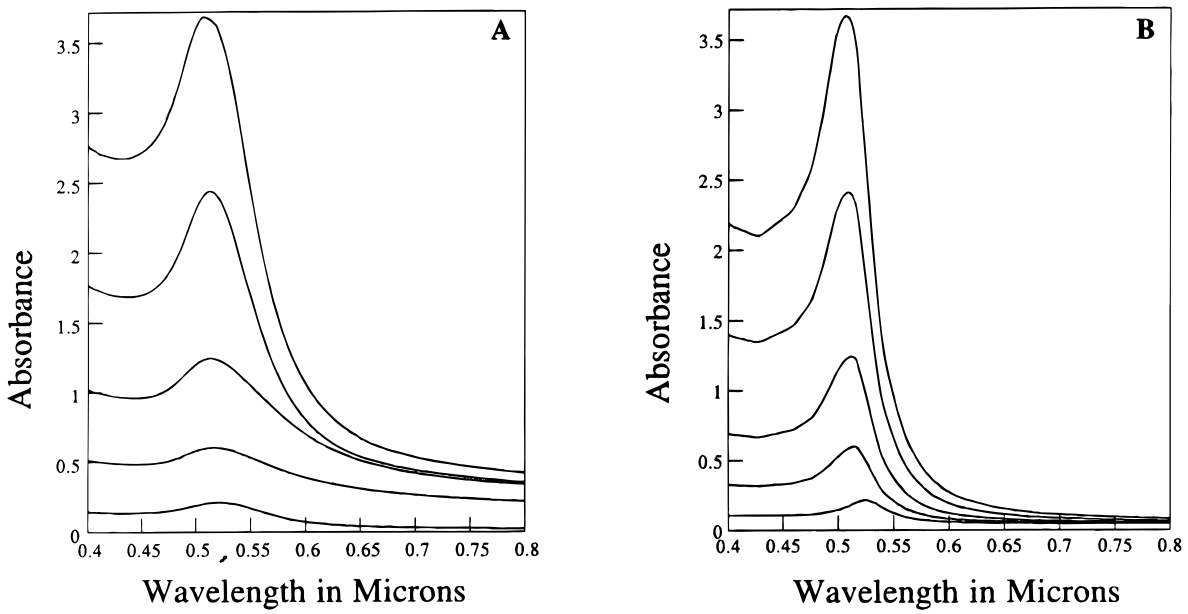

Figure 9. Experimental (A) and DMG-simulated (B) absorption spectra for membranes containing 22 nm diameter Au nanoparticles. Particles with five different aspect ratios (Table 2) are shown. The uppermost curve is for the highest aspect ratio nanoparticle, and the lowermost curve is for the lowest aspect ratio nanoparticle.

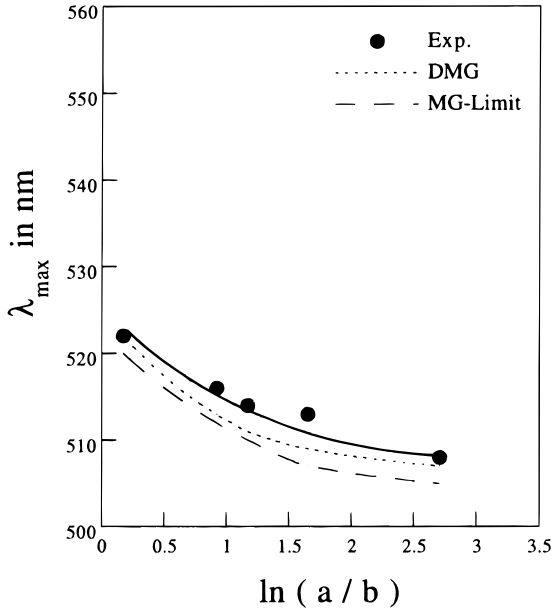

Figure 10. Plot of λ_{max} for experimental and simulated absorption spectra vs natural logarithm of the aspect ratio of the Au nanoparticle. The aspect ratio is defined as a/b, where a is the length and b is the diameter of the nanoparticle. These data are for 22 nm diameter nanoparticles. The experimental data are in bold (with data points). The DMG-simulated results are the dotted curve. The MG-simulated results are the dashed curve.

as would be expected from the high optical transparency of these membranes. The k_0 values for the sulfuric-acid-prepared membranes are lower and are independent of wavelength. The k_0 values for the oxalic-acid-prepared membranes are higher and decrease with increasing wavelength. The n_0 values for both types of membranes were found to be independent of wavelength. The average n_0 value for the oxalic-acid-prepared films over the wavelength range of interest here was 1.50. The average n_0 value for sulfuric-acid-prepared films was 1.54.

TEMs of the Gold Nanoparticles. Figure 4 shows TEM images of Au nanoparticles with three different aspect ratios that were prepared in the membrane with 52 nm diameter pores. The lengths, diameters, aspect ratios, and static screening parameters[2b] for all of the Au nanoparticles studied here are shown in Table 2.

Experimental and Simulated Absorption Spectra. Experimental optical absorption spectra for the composite membranes containing the 52 nm diameter Au nanoparticles are shown in Figure 5A. The uppermost spectrum is for the highest aspect ratio particles (Table 2), and the lowermost spectrum is for the lowest aspect ratio particles. As would be expected,[2a,b] the intensity of the plasmon resonance band increases, and λ_{max} decreases, with increasing aspect ratio (a/b, where a is the length and b is the diameter of the Au nanoparticle). As a result of this shift in λ_{max}, the color of these composites change with aspect ratio. When illuminated from behind with a tungsten source, the aspect ratio (a/b) = 1.3 composite (bottom curve in Figure 5A) displayed a blue-purplish hue (λ_{max} = 540 nm). The membranes containing the highest aspect ratio particles appeared red (λ_{max} = 518 nm).

DMG-simulated absorption spectra for composites containing Au nanocylinders of these dimensions are shown in Figure 5B. The only adjustable parameter in these simulations is the thickness of the optical layer,[2b,c] and this parameter affects only the absolute absorption intensity. That is, λ_{max} and the general shape of the band are not influenced by the magnitude of this adjustable parameter. Rather, these characteristics of the absorption spectrum are determined by the nonadjustable input parameters, which are the length and diameter of the nanoparticle and the optical constants of the metal and the alumina.

The agreement between the experimental and simulated spectra is, qualitatively, good. The shape of the band is faithfully reproduced; however, the widths of the experimental bands are greater than the simulated bands. The broadening in the experimental spectra is due to the finite distribution in both the length and diameter of the particles (Table 2). Kreibig and Vollmer have suggested approaches for modeling this inhomogeneous broadening.[11] Most importantly, in agreement with the experimental spectra, the simulated spectra show a blue-shift in λ_{max} with increasing aspect ratio.

We are especially interested in the extent of agreement between the experimental and simulated λ_{max} values. This interest stems from our previous work on Au nanoparticles that had larger diameters than those investigated here.[2a,b] We found

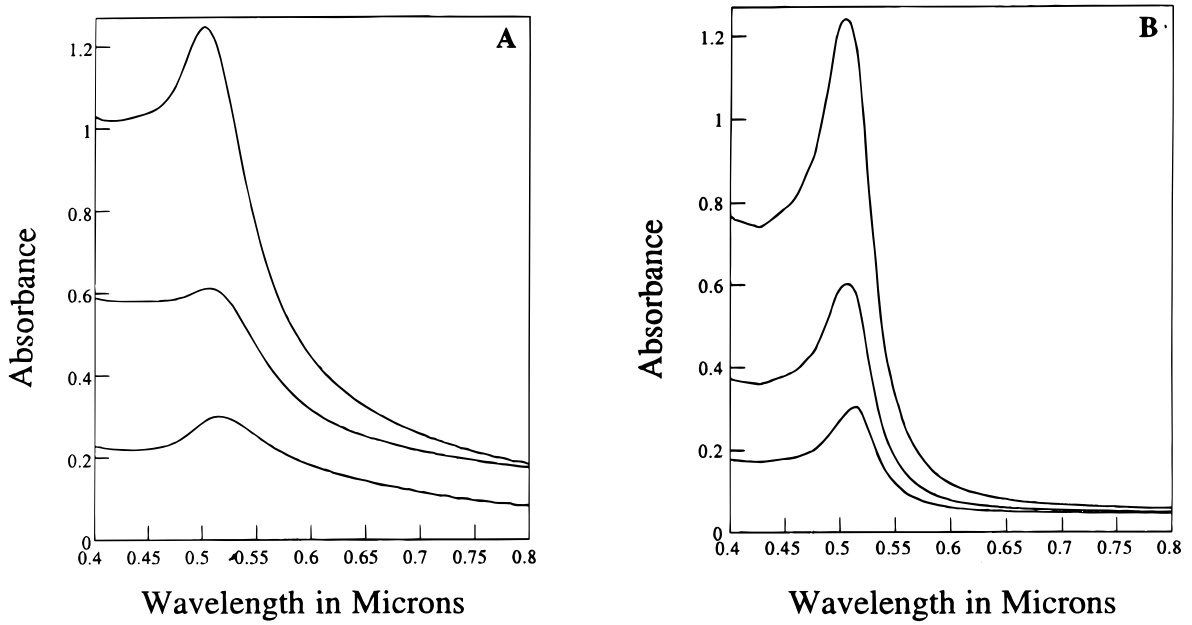

Figure 11. Experimental (A) and DMG-simulated (B) absorption spectra for membranes containing 16 nm diameter Au nanoparticles. Particles with three different aspect ratios (Table 2) are shown. The uppermost curve is for the highest aspect ratio nanoparticle, and the lowermost curve is for the lowest aspect ratio nanoparticle.

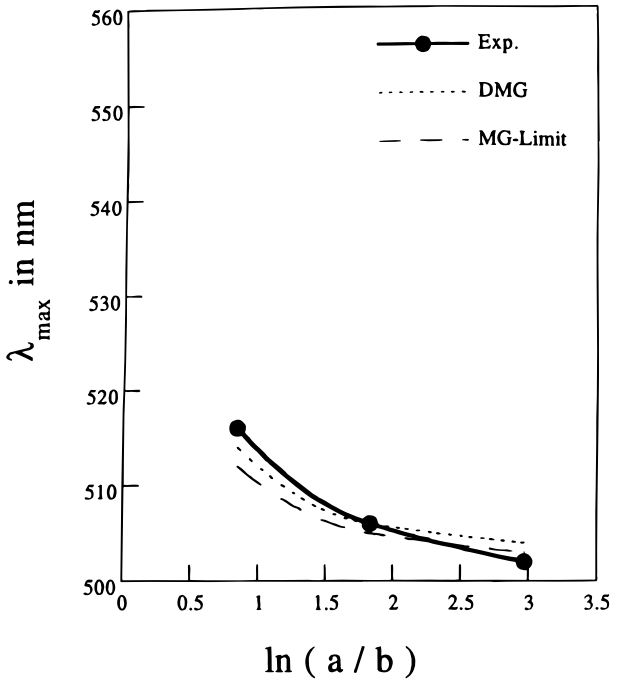

Figure 12. Plot of λ_{max} for experimental and simulated absorption spectra vs natural logarithm of the aspect ratio of the Au nanoparticle. The aspect ratio is defined as a/b, where a is the length and b is the diameter of the nanoparticle. These data are for 16 nm diameter nanoparticles. The experimental data are in bold (with data points). The DMG-simulated results are the dotted curve. The MG-simulated results are the dashed curve.

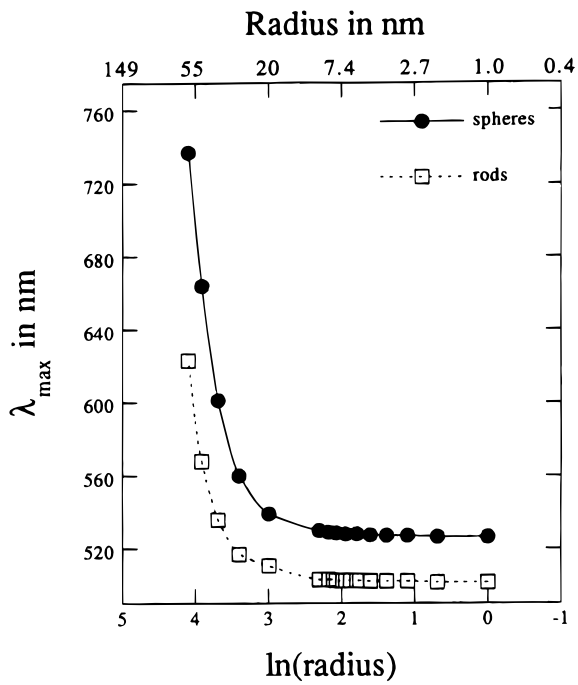

Figure 13. Plot of λ_{max} for DMG-simulated spectra vs the natural logarithm of the radius of the nanoparticle in the composite. The upper curve assumes spherical nanoparticles. The lower curve assumes long, needlelike particles (aspect ratio = 100).

that λ_{max} values blue-shifted with decreasing nanoparticle diameter but that λ_{max} values for all of the particles investigated were significantly larger than values predicted by the conventional (i.e., quasi-static) MG theory. Hence, the quasi-static MG theory can be viewed as a limiting case in the optical properties of nanometals. One of the objectives of the current study was to see if nanoparticles with small enough diameters to achieve this limiting case could be prepared.

Figure 6 shows both the experimental and simulated (MG and DMG) variation in λ_{max} with aspect ratio for the 52 nm diameter Au nanoparticles. As would be expected for such large-diameter particles,[2b] the λ_{max} values predicted by conventional quasi-static MG theory, bottom curve, are significantly smaller than the experimental λ_{max} values. The DMG theory does a much better job of predicting the experimental λ_{max} values. Experimental optical absorption spectra for the Au/alumina composite membranes containing the 32 nm diameter Au nanoparticles are shown in Figure 7A. Spectra for nanocylinders having six different aspect ratios are shown. Again, we see the characteristic increase in absorption intensity and a decrease in λ_{max}, with increasing aspect ratio. The color of these membranes proceeded from bluish-purple (a/b = 1.0, λ_{max} = 539 nm) through various red hues and finally to orange-red (a/b = 12, λ_{max} = 508 nm).

Simulated (DMG) absorption spectra for composites containing Au nanoparticles of these dimensions are shown in Figure 7B. The agreement between the experimental and simulated spectra is, again, qualitatively, quite good. Figure 8 shows both the experimental and simulated variation in λ_{max} with nanoparticle aspect ratio for the membranes containing the 32 nm diameter Au particles. In this case, the agreement between the experimental and DMG-simulated λ_{max} values is better than for the larger diameter particles discussed above (Figure 6). Furthermore, a comparison with the curve obtained from the quasi-static MG simulation, the lowest curve in Figure 8, clearly shows that these smaller diameter particles are approaching the quasi-static regime.

Experimental optical absorption spectra for the Au/alumina composite membranes containing the 22 nm diameter Au nanoparticles are shown in Figure 9A. Again, we see the characteristic changes in intensity and position of the spectra with aspect ratio. The colors of these membranes proceeded from bright ruby-pink ($a/b = 1.2$, $\lambda_{max} = 522$ nm) to various reddish hues and finally to orange-red ($a/b = 14$, $\lambda_{max} = 508$ nm). The corresponding DMG-smulated spectra are shown in Figure 9B. Figure 10 shows both the experimental and simulated variation in λ_{max} with nanoparticle aspect ratio. Note that the MG and DMG simulations now give very similar λ_{max} values. This indicates that the diameter of these particles (22 nm) is sufficiently small that the quasi-static limit is being approached. The experimental λ_{max} values are essentially identical with the values produced by the DMG simulation.

Experimental and simulated optical absorption spectra for the Au/alumina composite membranes containing the smallest (16 nm) diameter Au nanocylinders are shown in Figure 11. The agreement between the experimental and simulated spectra is reasonably good. However, the experimental peaks are not as well-defined as in the spectra for the larger diameter particles. This is due to the lower absolute absorption intensity for these very small diameter particles. Finally, Figure 12 shows both the experimental and simulated variation in λ_{max} with nanoparticle aspect ratio. The experimental and simulated (both MG and DMG) λ_{max} values are now all essentially identical. This indicates that the quasi-static limit has been achieved for these 16 nm diameter Au nanoparticles.

Conclusions

The above results suggest that the quasi-static MG limit is achieved for Au nanoparticles with radii of 8 nm or less. To explore this result theoretically, we used the DMG theory to calculate λ_{max} as a function of particle radius, for spherical and long, needlelike Au nanoparticles. The results of these calculations are shown in Figure 13. In agreement with the experimental data, λ_{max} for both the spherical particles (upper curve) and needlelike particles (lower curve) initially decrease with decreasing particle radius. However, at sufficiently small radius, λ_{max} reaches a lower limit and shows no further change with radius. This lower limit is the quasi-static limit. In agreement with the experimental data obtained here, these calculations show that this quasi-static limit is achieved for particles with radii of ca. 7.5 nm or smaller.

Acknowledgment. This work was supported by the Office of Naval Research. We also acknowledge the Colorado State University Electron Microscopy Center.

References and Notes

(1) Martin, C. R. *Science* **1994**, *266*, 1961.

(2) (a) Foss, C. A., Jr.; Hornyak, G. L.; Stockert, J. A.; Martin, C. R. *J. Phys. Chem.* **1992**, *96*, 7497. (b) Foss, C. A., Jr.; Hornyak, G. L.; Stockert, J. A.; Martin, C. R. *J. Phys. Chem.* **1994**, *98*, 2963. (c) Foss, C. A., Jr.; Tierney, M. J.; Martin, C. R. *J. Phys. Chem.* **1992**, *96*, 9001.

(3) (a) Preston, C. K.; Moskovits, M. J. *J. Phys. Chem.* **1993**, *97*, 8405. (b) Preston, C. K.; Moskovits, M. J. *J. Phys. Chem.* **1988**, *92*, 2957. (c) Huber, C. A.; Huber, T. E.; Sadoqi, M.; Lubin, J. A.; Manelis, S.; Prater, C. B. *Science* **1994**, *263*, 800. (d) Masuda, H.; Kazuyuki, N.; Noboyushi, B. *Thin Solid Films* **1993**, *223*, 1. (e) Masuda, H.; Tanaka, H.; Noboyushi, B. *Chem. Lett.* **1990**, 621. (f) Blondel, A.; Meier, J. P.; Doudin, B; Ansermet, J.-Ph. *Appl. Phys. Lett.* **1994**, *65*, 3019. (g) Moskovits, M. U.S. Patent, 5,202,290, 1993. (h) Ohji, N.; Enomoto, N.; Mizushima, T.; Noriyoshi, K.; Morioka, Y.; Ueno, A. *J. Chem. Soc., Faraday Trans.* **1994**, *90*, 1279. (i) Masuda, H.; Fukuda, K. *Science* **1995**, *268*, 1466.

(4) (a) Diggel, J. W.; Downie, T. C.; Goulding, C. W. *Chem. Rev.* **1969**, *69*, 365. (b) Keller, F.; Hunter, M. S.; Robinson, D. L. *J. Electrochem. Soc.* **1953**, *100*, 411. (c) Furneaux, R. C.; Rigby, W. R.; Davidson, A. P. *Nature* **1980**, *337*, 147. (d) Thompson, G. E.; Wood, G. C. In *Treatise on Materials Science and Technology*; Scully, J. C., Ed.; Academic Press: New York, 1983; Vol. 23. (e) Wittmann, Z.; Kantor, E.; Belafi, L.; Farkas, L. P. *Talanta* **1992**, *39*, 1583. (f) Wefers, K.; Misra, C. *Oxides and Hydroxides of Aluminum*; Alcoa Technical Paper No. 19, revised, Alcoa Laboratories, 1987.

(5) Miller, C. J., Microporous Aluminum Oxide Films at Electrodes Ph.D. Dissertation, University of California at Berkeley, 1987, U.M. Dissertation Service.

(6) Furneaux, R. C.; Rigby, W. R.; Davidson, A. P. U.S. Patent No. 4,687, 551, 1987.

(7) Hornyak, G. L. Optical Properties of Nanometal-Porous Alumina Composites. Ph.D. Dissertation, Colorado State University, Fort Collins, CO, 1997.

(8) Thèye, M.-L. *Phys. Rev. B.* **1970**, *8*, 3060.

(9) (a) Maxwell−Garnett, J. C. *Philos. Trans. R. Soc. London A* **1904**, *203*, 385. (b) Maxwell−Garnett, J. C. *Philos. Trans. R. Soc. London A* **1906**, *205*, 247.

(10) Aspnes, D. E. *Thin Solid Films* **1982**, *89*, 249.

(11) Kreibig, U.; Vollmer, M. *Optical Properties of Metal Clusters*; Springer- Verlag, New York, 1995.

(12) (a) Granqvist, C. G.; Hunderi, O. *Phys. Rev. B* **1977**, *16*, 3513. (b) Heller, A; Aspnes, D. E.; Porter, J. D.; Sheng, T. T.; Vadimsky, R. G. *J. Phys. Chem.* **1985**, *89*, 4444.

(13) Kreibig, U.; Althoff, A.; Pressman, H. *Surf. Sci.* **1981**, *106*, 308.

(14) (a) Meier, M.; Wokaun, A. *Opt. Lett.* **1983**, *8*, 581. (b) Zeman, E. J.; Schatz, G. C. *J. Phys. Chem.* **1987**, *91*, 634.

(15) Bruggeman, D. A. *Ann. Phys. (Leipzig)* **1935**, *24*, 636.

(16) (a) Parkhutik, V. P.; Shershulsky, S. *J. Phys. D: Appl. Phys.* **1992**, *25*, 1258. (b) Patermarakis, G.; Lenas, P.; Karavassilis, C. H.; Papayinnis, G. *Electrochim. Acta* **1993**, *38*, 2351. (c) Patermarakis, G.; Moussoutzanis, K. *J. Electrochem. Soc.* **1995**, *142*, 737.